Title: Thread-stripping test procedures leading to factors of safety data for friction-drilled holes in thin-section aluminium alloy

Authors: Hao Wu[1], Ryan Clarke[1,2], Mark Porter[1,3], Richard Ward[1], Justin Quinn[1], Cormac McGarrigle[1], Shaun McFadden[1]

Affiliations:

[1]School of Computing, Engineering, and Intelligent Systems, Ulster University, Magee Campus, Derry, Northern Ireland, UK, BT48 7JL

[2]Linamar Light Metals Belfast, City Business Park, Dunmurry, Belfast, Northern Ireland, UK, BT17 9HN (present address)

[3]Letterkenny Institute of Technology, Letterkenny, Co. Donegal, Republic of Ireland (present address)

Correspondence to: Shaun McFadden (s.mcfadden2@ulster.ac.uk)

Abstract

Friction drilling is a hole-making process suitable for thin sections of ductile metal. A rotating tool is plunged into the workpiece to form the pilot hole. The hole is then threaded in a follow-up process. A bushing forms on the exit side of the hole, which allows for longer engagement lengths in threaded assemblies. For comparison purposes, four combinations of threaded-hole processes were applied to 1.5mm-section, 6082-T6 aluminium alloy. The processes involved were friction and twist drilling followed by thread forming or cutting. Vickers hardness and microstructural analyses were used to assess the condition of the material. An in-house test method was developed to measure the axial load-deflection response. Progressive failure occurred by thread stripping. Friction drilling followed by thread forming gave peak loads 35% higher than conventionally drilled and tapped holes. Also, hardness increased from 111HV in the parent metal to 125HV (with an increase in hardness to depths of 0.5mm) due to work hardening. Evidence of precipitate dissolution was negligible which suggests that the friction drilling process operated below the solvus temperature. A novel approach for determining reliably-based, thread-stripping Factors of Safety (*FoS*) is presented. *FoS* in the range 3.61 to 4.38 gave a reliability of 95% to 99.9% against thread stripping in friction-drilled, thread formed joints.

Keywords: Friction drilling; Thread forming; Twist drilling; Thread cutting; Microstructure; Mechanical properties

1. Introduction

Threaded holes in thin-section materials are often unsatisfactory because the engagement length of the thread can be too short. If the hole is made by conventional subtractive manufacturing processes, such as twist drilling, then the engagement length of any subsequent thread is limited to the section's thickness. If the thread's pitch is of similar magnitude to the thickness of the section, then too few complete threads exist within the hole. Hence, the threaded assembly is prone to thread stripping under axial load.

Friction drilling, patented by van Geffen [1] is a hole-making processes that does not remove material but instead creates the hole by solid-state deformation. It is also known as form drilling or flow drilling. In friction drilling, a rotating conical tool is plunged into the workpiece. Frictional heat is generated that then softens the material and causes the metal to flow as the rotating tool is plunged into the metal. The resulting flow of material creates a bushing on the exit side of the hole. This bushing gives an improved geometry, specifically, longer engagement lengths, for threaded assemblies when compared to conventional drilling.

There are other advantages to friction drilling over conventional twist drilling. No material is removed during the friction drilling process; hence, no chips (also known as swarf) are built up and, therefore, no troublesome entanglement occurs. No cutting fluid is required. Hence, the process is considered quick, clean, and dry. Since friction drills are short and stiff, they exhibit good centre-point precision; unlike conventional twist drills, which can wander unless a pilot hole or punch mark with the required

positional accuracy is created first.

Kumar and Hynes [2] have presented a review of friction drilling for sheet metal applications across various metals and alloys. Clear examples of industrial application are included, for example, automotive bodywork, tubular framework found in furniture, and thin-walled pressure vessels (in particular a fire extinguisher canister). Other cited applications areas [2] include heating and ventilation pipework, thin section components for the built environment (construction), and agriculture applications. However, their review focuses on the friction drilling process with an introductory review of thread making.

Threaded holes are essential standard elements in many structural components. Design guidelines for these standard threads are well document. Budynas and Nisbett [3] provide design guidelines in the revised version of the classic textbook Shigley's Mechanical Engineering Design. Oberg et al. [4] provide an overview of thread stripping along with a comprehensive review of standard thread geometries and tolerance grade information. Juvinall and Marshek [5] provide general guidelines for designing threaded fasteners. However, there is no specific consideration in any of the design manuals given to threaded joints made by friction drilling. This gap in knowledge needs to be addressed if friction drilling is to become more widely accepted for threaded joints in thin-walled structures.

Since friction drilling creates an internal thread in ductile metals, thread stripping is an issue, especially when the bolts used to transfer the loads are made from harder materials. Standards organisation ISO [6] and ASTM [7] provide details of

thread-strip tests where designated proof loads are applied by pushing (or pulling) a threaded mandrel against an internally threaded nut. The nut is expected to avoid stripping or rupture during loading and, afterwards, must be removable by hand (or started with a half turn with a wrench and then removed by hand). This type of pass/fail test, while useful in its simplicity, is limited in its scientific value. Furthermore, the standard tests are limited to standard nuts and specific materials under specified material conditions (e.g., ISO is limited to steels). The standard tests have limited applicability to the testing of friction-drilled, threaded joints in thin-walled materials.

1.1 Literature review

A significant body of work is available that focusses on the friction drilling process in various materials. Miller et al. [8] have studied the temperatures and forces developed during friction drilling of AISI 1020 cold-rolled carbon steel. Peak temperatures up to 700ºC were reported. Additionally, Miller et al. [9] presented on the application of the friction drilling process to cast aluminium alloy (Al380) and cast magnesium alloy (MgAZ91D) where a preheating process was developed to improve the metal flow characteristic. Miller and Shih [10] developed a 3D Finite Element Model (FEM) with temperature dependent properties and an adaptive mesh. A coefficient of friction of 0.7 is reported for the drilling process. The thermo-mechanical FEM has been shown to predict a peak temperature of 580ºC when drilling aluminium 6061-T6 alloy. These studies represent a comprehensive body of work on friction flow drilling in metals; however, the analysis of threaded friction drilled holes is not covered extensively.

Chow et al. [11] reported on investigations in friction drilling of austenitic stainless steel AISI304 using a sintered carbide tool and have compared results to those using a tungsten carbide tool. In their study, the Taguchi method was used to optimise the performance. A particular focus was placed on improving the surface finish and improving geometry. Ozek and Demir [12] have reported on investigations on the performance of friction drilling across a range of aluminium alloys (1050, 6061, 5083, 7075). Temperature data close to each hole were reported. Bushing formation, surface finish and bushing length have all been reviewed and optimal parameters are reported for each case. Hynes and Kumar [13] presented a Taguchi method to optimise the bushing length on galvanised steel used in boat making. They showed that bushing length is linked to process variables such as tool rotation rate, tool angle and workpiece thickness.

As with other hot working processes, recrystallization and dissolution of the second phase particles can occur during friction drilling if the temperatures are sufficient. Eliseev et al. [14] reported that when friction drilling was applied to 2024 aluminium alloy, recrystallisation and dissolution of incoherent second phase particles occurred. It was demonstrated that the hardness values in the recrystallized material increased; however, the temper condition of the parent metal, whether it was peak aged or not, was unclear. Miller et al. [15] have shown the versatility of the friction drilling process by applying it to four metals, namely, two steel grades (AISI 1020 and 4130), a wrought aluminium alloy (5052), and a commercially pure titanium. In all cases, the final friction drilled components were analysed for their geometry and microstructural

features. Microhardness data were presented for areas within the Thermo-Mechanically Affected Zones (TMAZ). In their study, it has been reported that only AISI 4130 shows a clear modification in the hardness readings in the vicinity of the hole – the hardness levels were reported to increase in the TMAZ.

Recently, Hamzawy et al. [16] reported friction drilling results for age-hardenable wrought aluminium alloys 6082 and 7075. Thermal response was measured and it has been found that the peak processing temperatures are typically between 220ºC and 380ºC, which is in the range of the artificial age hardening temperatures for 6082 but below the solution annealing (solvus) temperature of approximately 550ºC for that alloy.

Limited information is available on testing the mechanical performance of assembled joints. Urbikain et al. [17] studied the joining of dissimilar metals, aluminium alloys AISI 1045 with 304 stainless steel, by friction drilling and twist drilling. They tested the mechanical properties of the joints by pulling the two joined sheets apart. As a result, the main failure mode in the reported case was shearing or tearing of the sheet rather than thread stripping. Wittke et al. [18] investigated thread stripping in friction drilled cast magnesium alloy AZ91. Load testing (quasi-static) and cyclical fatigue testing were studied on two batches: one with and the other without pre-heating of the tool. The quasi-static testing results showed that the load increased in a linear-elastic fashion up to a maximum value and then failed progressively. They also reported no difference in thread performance due to the pre-heating the tool. This work (Wittke and co-workers) is one of the few cases in literature that reports on thread stripping in

friction drilled and threaded holes. However, their study, while interesting and novel, provides limited information for designers in terms of the Factor of Safety to use when the selecting the load rating of the joint.

There are several other solid-state forming processes of interest that are similar to friction drilling, such as Friction Stir Welding (FSW) [19,20] and other process variants [21,22]. These processes are known to affect the condition of the material creating Heat Affected Zones (HAZ) and TMAZ. These temperatures developed depend on friction, tool speed, feed rate, tool geometry, and time in contact with the sample. Friction drilling is fast in-out process and so temperatures are expected to be lower than in FSW processes. Nevertheless, interesting comparisons can be made between friction drilling process and FSW.

1.2 Aims and objectives

Although previous studies have covered a range of investigations on friction drilling, it is difficult to find direct comparison of the friction drilling to conventional material removal process. In addition, there is very little information on how results from mechanical testing of friction-drilled threaded holes are translated into design factors (to Factors of Safety). This manuscript aims to investigate the mechanical performance of internal screw threads where the hole is made by friction drilling in 6082-T6 aluminium alloy as an exemplar. The objectives of this study can be summarised as follows:

- To compare the manufacture of threaded holes in thin-walled aluminium using combinations of manufacturing processes. The combinations include friction

drilling and conventional twist drilling to make the starting hole, followed by thread forming and cutting to make the internal thread (four combinations).

- To investigate any localised material property changes in 6082-T6 as a result of the drilling and threading processes.
- To generate test data on the axial load-bearing capacity for all four combinations of threaded-hole processes.
- To translate the test data into reliability-based Factors of Safety to safeguard against internal thread stripping in thin-walled structures.

The materials and methods section describes the experimental testing and analysis procedures. The procedures to establish the design factors are also presented. A results section describes the findings and a discussion section is provided to provide greater insight into the results. Finally a conclusion section is provided that summarises the outcomes achieved in the investigation.

2. Materials and methods

2.1 Workpiece material

The workpiece material used in this study, Al-Mg-Si alloy 6082-T6, was sourced in the form of 25mm extruded box section (hollow profile) with a nominal uniform wall thickness of 1.5mm. Samples were initially cut to a length of 70mm. Table 1 provides standard properties for 6082-T6. The properties referenced here are minimum standard values for hollow extruded profiles with wall thickness less than 5mm.

Table 1. Minimum material properties of aluminium alloy 6082-T6 (hollow profile).

Density, $g \cdot cm^{-3}$	Proof stress, MPa	Tensile strength, MPa	Elongation, %	Hardness, HBW[a] (HV conversion)[b]
2.7	250	290	8	95 (111)

[a] quoted in [23] for reference only.
[b] converted from HBW to HV based on a conversion for aluminium alloys [24].

In Al-Mg-Si alloys, the main strengthening mechanism is precipitation strengthening (solid solution treatment followed by quench and artificial aging). From solid solution a series of precipitation stages occur which ultimately lead to a stable β-Mg_2Si phase with a size in the range of 10 to 20μm [25].

2.2 Tooling details

Fig. 1 (a) shows a schematic diagram of the friction drill and thread forming tools. Fig. 1 (b) shows all four tools used in the investigation: friction drill, twist drill, thread forming, and thread cutting (or taper tapping). The friction drilling tool is commercially available with a pin diameter of 7.1mm. The high-speed steel twist drill had a diameter of 6.8mm. The thread forming tool had a conical tip and five narrow, straight flutes for lubrication purposes along the axis. The thread cutting tool (or taper tapping tool) had four large flutes which allow the metal chips to escape from the hole during the thread-cutting process. The thread designation was M8×1.25 throughout, which is a standard metric coarse thread.

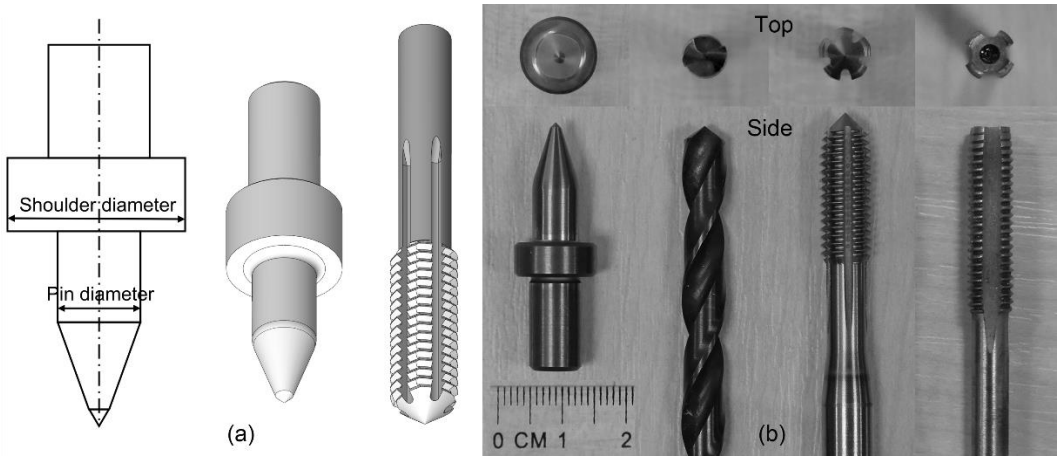

Fig. 1. (a) Schematic of the friction drilling and thread forming tools. (b) Plan view (top row) and side view (bottom row) of the tools used for (from left to right) friction drilling, twist drilling, thread forming and thread cutting, respectively.

2.3 Threaded-hole production

A vertical axis Haas CNC milling machine with an automatic tool changer was used to drill and thread all holes. As mentioned, four tools were available, which allowed for four process combinations. The combinations of drilling and tapping processes were designated S1 to S4. The tools pairs and process parameters for each combination are listed in Table 2. Process parameters used throughout were based on recommended feeds and speeds. A lubricant paste was applied to all processes. In all cases the tools were retracted from the workpiece immediately, that is, there was no dwell time during the drilling or tapping operation, thereby reducing heat input.

After the threaded holes were made, the hollow box sections were cut along their axial direction to form C-sections (with the threaded hole positioned in the centre of the largest surface).

Table 2. Details of tool pairings and process parameters for each scenario.

Scenario	Process	Rotation rate,	Feed rate,

number	description	RPM	$mm \cdot min^{-1}$
S1	Friction drilling	3000	270
	Thread forming	750	937.5
S2	Friction drilling	3000	270
	Thread cutting	800	1000
S3	Twist drilling	2580	200
	Thread forming	750	937.5
S4	Twist drilling	2580	200
	Thread cutting	800	1000

2.4 Experimental preparation, measurement, and mechanical testing

2.4.1 Microstructure and micro hardness preparation

Representative samples from each scenario were prepared for microstructure and Vickers hardness testing. Additionally, one sample that was friction drilled only (i.e., with no thread making process applied) and prepared for analysis. The sample preparation process involved abrasive cutting along the diametral plane and casting in a cold-mount epoxy resin. The samples were polished on a semi-automatic polisher through incremental stages of silicon carbide grinding papers, to diamond suspension of 3μm, and then finished using a 0.06μm colloidal silica suspension.

Vickers hardness was performed using a Future-tech micro-hardness tester with, a 500g load and a 10 seconds holding time. A day-of-use verification check was performed on a calibrated HV700 test block and results were found to be within

acceptable standard bias levels [26]. The hardness maps were made under the principle that each test point was kept at least 0.25mm away from any edges or neighbouring test points. Samples were then etched by swabbing with Keller's reagent for microscopy imaging.

2.4.2 Bushing measurement

A consistent procedure was used to estimate the engagement length of the thread. In each case, the drilled and threaded component was placed on a flat (ground) measuring plate with the hole's entry surface (i.e., upper surface) facing down. A traditional micrometer (T-shaped) depth gauge was used to measure the full linear dimension from the flat surface to the highest point on the bushing. While in contact with bushing, the base on the depth gauge was kept parallel to the measuring surface so that the retractable measuring rod stayed perpendicular to the measuring surface and parallel to the hole's axis. The extension length of the measuring rod was then used as an estimate of engagement length, L_e.

2.4.3 Mechanical thread stripping tests

A work-holding fixture (Fig. 2 (a)) was specifically designed and installed on an INSTRON 5500R universal tester setup in compression mode (Fig. 2 (b)). Crosshead speed was set to 2mm/min. As illustrated in Fig. 2 (a) and (b), the threaded hole in the C-section sample received a threaded steel bolt (M8×1.25mm hex-head), loosely inserted to a depth of 15mm.

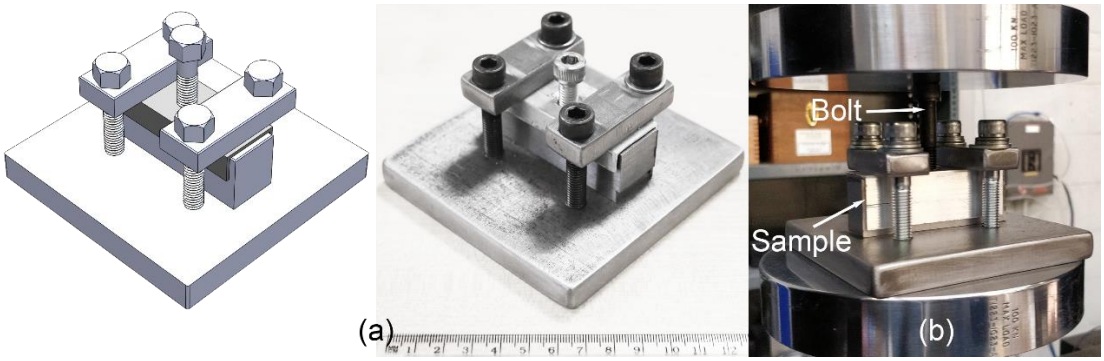

Fig. 2. (a) Schematic (left) and actual images (right) of the work-holding fixture and (b) the fixture in position on the universal tester.

Fig. 3 shows a detailed cross-section view of the work-holding fixture. The retaining structure (consisting of two retaining bolts and a cross member), visible in the background, did not interfere with the test process. This is one of two retaining structures as shown in Fig. 2. The hatched cross-sectional areas in Fig. 3 give insight as to how the sample was loaded. When a compressive load is applied on the top of the M8×1.25 bolt, that load is transferred to the threads in the sample and reacted by the anvil on the underside of the sample. The anvil had a clearance hole with sufficient distance (approx. 1mm) for both bushing and bolt to pass through and to ensure that shear loads were transferred from the bolt to the sample via the threads.

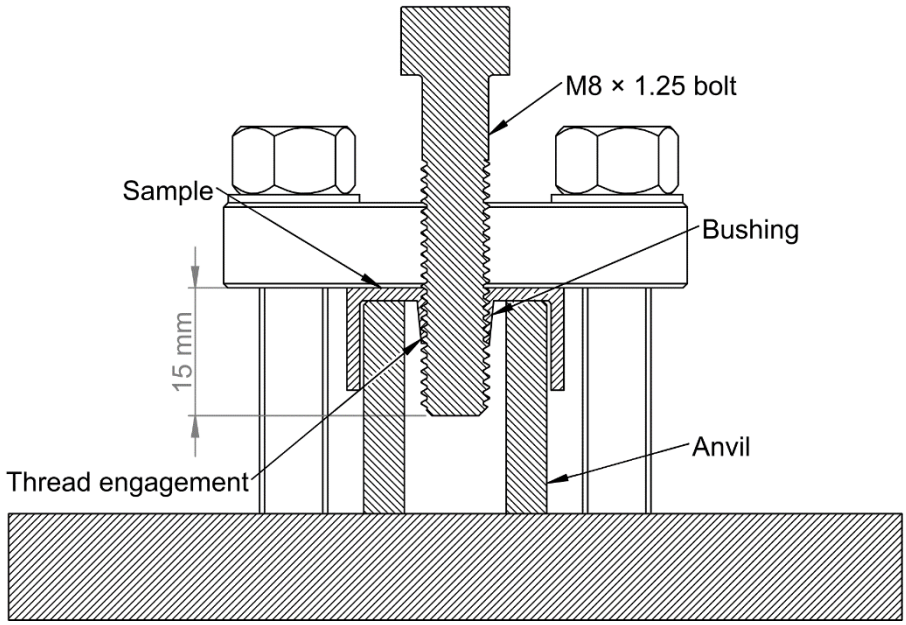

Fig. 3. Cross-section of the work holding fixture with sample and load bolt in situ.

The anvil had overall dimensions of 22×22×70 mm and was fixed to the centre of the base plate (Fig. 2 (a)). The loads and deflections were recorded using a calibrated test cell. Hence, load-deflection data were plotted and peak loads on each curve were recorded. Peak load was defined as the failure load, $F_{f,i}$ in each case. Six samples were tested to destruction for each scenario represented in Table 2 (giving 6×4 load-deflection data sets).

2.5 Calculation methods

2.5.1 Thread area calculations

Assuming that thread failure occurs by thread stripping, the shear stress on the threads must be calculated. To perform such calculations, the thread area must be calculated. The Machinery's handbook [4] provides standard data on the geometry of the thread

profiles. In particular, the thread geometry is needed to calculate the thread area for shear stress calculations. The thread area, A_n, is therefore given as

$$A_n = 25.4^2 \left[3.1416 n_p L_e D_{min} \left(\frac{1}{2n_p} + 0.57735\,(D_{min} - E_{max})\right)\right]. \quad (1)$$

where n_p is the number of threads per inch, L_e is the engagement length, D_{min} is the minimum major diameter of the external thread, and E_{max} is the maximum pitch of the internal thread. The term in square brackets, provided in [4], requires imperial units (inches). The factor 25.4^2 represents a unit conversion from inch^2 to mm^2. The values D_{min} and E_{max} are limits or threshold values based on the thread tolerance grades and therefore do vary. The values for D_{min} and E_{max} are based on a 6g6H tolerance grade, which gives D_{min} = 8.5719mm and E_{max} = 8.16mm. The value for threads per inch is determined from the thread pitch of 1.25mm (n_p = 20.32 inch^{-1}) and is assumed to be consistent (i.e., with negligible variance). The engagement length L_e is the parameter expected to have the largest variance, leading to variance in the shear area calculation.

2.5.2 Statistical considerations and calculations

As mentioned, load-deflection dataset were plotted and peak loads were defined as failure load, $F_{f,i}$ for each case. Because each scenario was tested with a sample size of six (n = 6), it was possible to generate statistical outputs. The absolute sample standard deviation for the failure loads in any given scenario is calculated as

$$S_{F_f} = \sqrt{\frac{\sum_{i=1}^{n}\left(F_{f,i} - \bar{F}_f\right)^2}{n-1}}. \quad (2)$$

where $\bar{F}_f$ is the mean value of failure load, and the relative standard deviation (or coefficient of variation) was given as

$$C_{F_f} = \frac{S_{F_f}}{\bar{F}_f}. \quad (3)$$

The sample standard error, which gives an estimate of the standard deviation of the mean failure value, was calculated in the usual way as

$$S_{\bar{F}_f} = \frac{S_{F_f}}{\sqrt{n}}. \quad (4)$$

The other main measured parameter, the engagement length L_e, was treated similarly:

$$S_{L_e} = \sqrt{\frac{\sum_{i=1}^{n}\left(L_{e,i}-\bar{L}_e\right)^2}{n-1}}. \quad (5)$$

$$C_{L_e} = \frac{S_{L_e}}{\bar{L}_e}. \quad (6)$$

$$S_{\bar{L}_e} = \frac{S_{L_e}}{\sqrt{n}}. \quad (7)$$

A two-factor analysis of variance (ANOVA) analysis was used to determine the statistical significances and interactions between the mean failure loads for the different hole drilling and thread cutting processes.

2.5.3 Stress calculations with statistical considerations

Several calculated parameters were derived from the measured values. The mean parameters were calculated in a deterministic way; hence, mean shear stress at failure, $\bar{\tau}_f$, is estimated as

$$\bar{\tau}_f = \bar{F}_f / \bar{A}_n. \quad (8)$$

where $\bar{A}_n$ is the mean shear area from Eqn. (1). This equation is based on the assumption that stress condition on the threads is pure shear.

The propagation of standard deviation in any calculated function $f(x,y)$ is given in general terms as

$$S_f = \sqrt{\left(\frac{\partial f}{\partial x}\right)^2 S_x^2 + \left(\frac{\partial f}{\partial y}\right)^2 S_y^2}. \quad (9)$$

So, in the case of shear area, A_n, standard deviation is related to the variance associated with the engagement length only. For shear area, Eqn. (9) is simplified to

$$S_{A_\mathrm{n}} = \bar{A}_\mathrm{n}\left(\frac{S_{\bar{L}_\mathrm{e}}}{\bar{L}_\mathrm{e}}\right). \tag{10}$$

Following reference [27], the equation for shear stress at failure (Eqn. (8)) follows the general form $f = b/a$ and the application of Eqn. (9) will give

$$S_{\tau_f} = \bar{\tau}\sqrt{\left(\frac{S_{F_f}}{\bar{F}_f}\right)^2 + \left(\frac{S_{A_\mathrm{n}}}{\bar{A}_\mathrm{n}}\right)^2 - 2\frac{S_{F_f,A_\mathrm{n}}}{\bar{F}_f\bar{A}_\mathrm{n}}}. \tag{11}$$

The function $S_{Ff,L\mathrm{e}}$ is the covariance and this is required in the case where failure loads and shear areas are correlated.

The corresponding relative standard deviations (coefficients of variances) for shear area and shear stress at failure can be defined as follows

$$C_{A_\mathrm{n}} = \frac{S_{A_\mathrm{n}}}{\bar{A}_\mathrm{n}}. \tag{12}$$

and

$$C_{\tau_f} = \frac{S_{\tau_f}}{\bar{\tau}_f}. \tag{13}$$

The preceding analysis is required to calculate the reliability and the design factors for a given level of reliability.

2.5.4 Reliability calculations leading to Factors of Safety

If an axial load, *F*, is applied to the threaded section then the corresponding applied shear stress in the internal thread follows

$$\tau = \frac{F}{A_\mathrm{n}}. \tag{14}$$

If this applied stress equals the mean-value of shear stress at failure, that is, if $\tau = \bar{\tau}_f$ then the reliability (*R*-value), against internal thread stripping is 50% (R = 0.5). Put simply, in any attempt to raise the applied stress level to the mean failure stress, $\tau = \bar{\tau}_f$, on average 50% of cases will fail before reaching that stress condition and 50% will have survived and could, in theory, be stressed to even higher levels. Hence, a

principal design factor, n_1, is defined as

$$n_1 = \frac{\tau_y}{\bar{\tau}_f}. \tag{15}$$

where τ_y is the shear yield strength. This principal design factor is interpreted as a design factor to ensure a reliability of 50% against internal thread stripping. It accounts for the imperfect geometry of the joint.

Shear yield strength is not provided in the materials standards but is derived from the normal yield strength, τ_y, using distortion energy theory [3]; hence,

$$\tau_y = 0.577\sigma_y. \tag{16}$$

In our case the minimum proof strength from EN-ISO 755 [23] will be used as a substitute for yield strength.

In most cases, a reliability of 50% is insufficient – reliability levels greater than 95% are routinely expected in design applications. Hence, the standardised *Z*-value is introduced and defined as

$$z = \frac{\tau - \bar{\tau}_f}{S_{\tau_f}}. \tag{17}$$

And a secondary design factor is defined as

$$n_2 = \frac{\bar{\tau}_f}{\tau}. \tag{18}$$

Rearranging Eqn. (17) and substituting with Eqn. (18) gives

$$n_2 = \frac{1}{Z\left(\frac{S_{\tau_f}}{\bar{\tau}_f}\right)+1} = \frac{1}{ZC_{\tau_f}+1}. \tag{19}$$

This secondary design factor gives a margin of safety based on the selected *Z*-value (where $Z \leq 0$). The *Z*-value is related to the reliability *R*-value through

$$R(Z) = 1 - \int_{-\infty}^{Z} \frac{1}{2u} exp\left(-\frac{u^2}{2}\right) du. \tag{20}$$

Here u is an intermediate integration variable. Eqn. (20) represents a one-sided area

calculation under a normalised Gaussian distribution. Standard statistical tables are available that correlate *R* values against *Z*-values [3]. For example, *Z* = -1.65 corresponds to *R* = 0.95, or 95% reliability.

Finally, the overall design Factor of Safety (*FoS*) is defined as the product of the design factors

$$FoS = n_1 n_2 = \frac{\tau_y}{\tau}. \quad (21)$$

This overall *FoS* relies on the principal design factor, n_1, to give a baseline of 50% reliability. Increased reliability is then achieved through the adjustment of n_2 calculated according to Eqn. (19) with the corresponding *Z*-value to give the required reliability.

The analysis presented so far only accounts for variance in the failure loads but does not account for variance in the applied load, which can occur in practice. In the case where variance is expected in the applied load then an inference calculation should be implemented. An approach for this situation is demonstrated later in this manuscript.

3. Results

3.1 Visual inspection after manufacture

Fig. 4 depicts typical representations of the threaded holes for each scenario after manufacture and before compression test. The upper row of images in Fig. 4 shows the upper surfaces where the drill tools entered the workpiece. Flashing was observed at the hole entry for S1 and S2 (due to upwards plastic flow of material to meet the tool shoulder). Holes produced by twist drilling had machining burrs (S3 and S4).

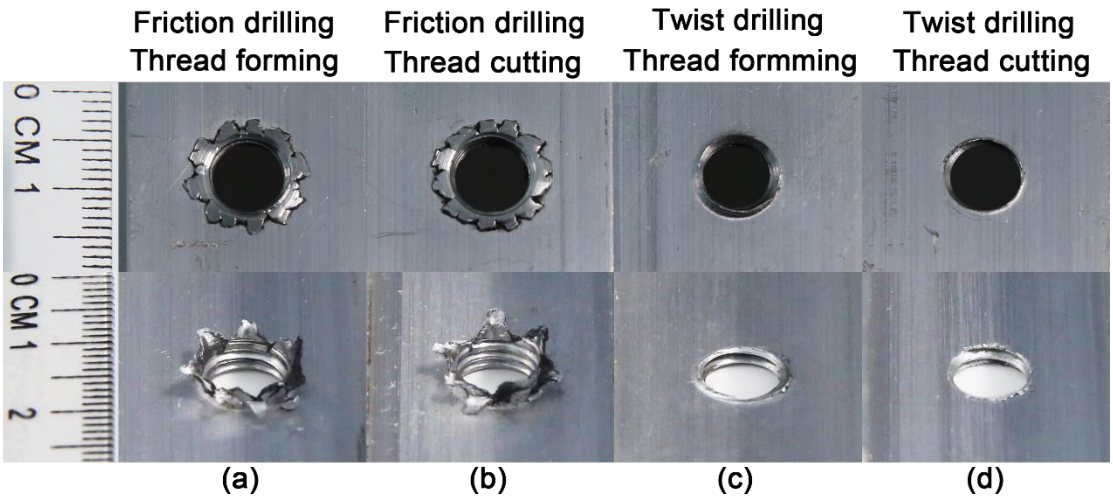

Fig. 4. Entry (top row) and exit (bottom row) features on holes produced in S1 (a), S2 (b), S3 (c), and S4 (d).

The bottom row of images in Fig. 4 show the underside where the drill tools exited. The holes produced by friction drilling had bushings with around 7 distinct petals (known as an exploded petal configuration). The petal formations are common in materials with low formability because of fissures forming in the bushing during the material deformation process [9]. As expected, no bushings were developed by twist drilling, instead burr formations were observed.

3.2 Cross sectional views and hardness maps

Fig. 5 shows the etched cross sections with Vickers hardness locations. The Vickers indents are colour coded according to the hardness value so that areas of increased hardness can be distinguished. In all cases the condition of the parent metal can be seen. The alloy 6082-T6 is supplied in the form of an extruded section and therefore shows a highly-deformed and aligned grain texture (flow lines) along the central axis. Low levels of Cr and Mn (within specification) in 6082 are known to retard recrystallization in deformed grain structures. There is an evidence of a limited

amount of recrystallization at the top and bottom surfaces to surface of the parent metal to depths of approx. 0.10 to 0.25mm; but, the material is not fully recrystallized. This partial recrystallization is typical for extruded section of 6082 [28].

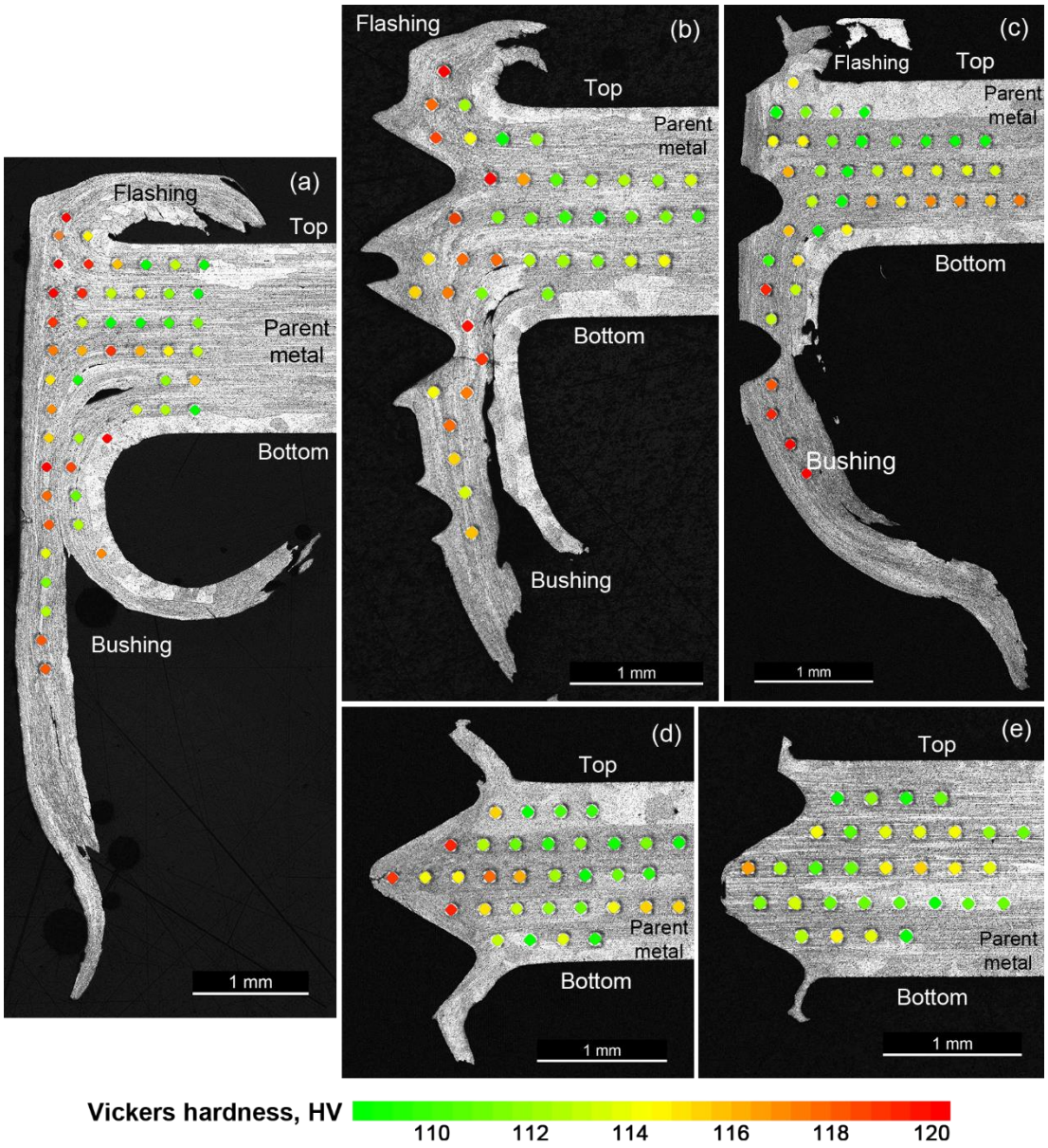

Fig. 5. Etched cross-sections (diametral plane) with hardness data: (a) hole made using friction drilling only and (b) (c) (d) and (e), threaded holes from S1, S2, S3 and S4, respectively.

Fig. 5 (a) shows a cross-section of a friction-drilled hole with no thread (drilled to the same specification as S1. Fig. 5 (b) and (c) show cross-sectional views of the friction-drilled and threaded holes using thread forming and thread cutting, respectively. The addendum (or thread's crown) on the formed thread (Fig. 5 (b)) showed horned features due to plastic flow. For the cut thread in Fig. 5 (c), the addendum is observed to have been truncated. Thread truncation is required to allow for clearance. Nominally, according to ISO 68 [29], addendums on internal threads are truncated by a length H/4 where H is the nominal peak-to-peak height of the thread. The addendum truncation on Fig. 5 (c) was outside specification for the ISO standard [29]. Due to the friction drill diameter being greater (7.1mm) than the recommended pilot hole diameter of 6.8mm. Fig. 5 (d) and (e) show the cross sections of the twist drilled holes threaded by thread forming and thread cutting, respectively. In line with the initial visual inspection, burr formations were evident. Thread geometry was within ISO specification for these two scenarios.

Fig. 6 shows the microstructures at higher magnifications of the same scenarios represented in Fig. 5. Red arrows represent feature that are shown at higher magnification levels. Thermo-Mechanically Affected Zones or TMAZ (where they exist) are identified by examining the flow lines. Flow lines in the parent metal are parallel in the axial direction. Where flow lines diverge shows the extent of the TMAZ. Keller's reagent reveals the presence of coarse β-Mg_2Si precipitates (seen a black particles < 10μm). Interestingly, these particles are well distributed throughout

and exist all the way to the machined surfaces. They have not been diminished in number due to the process. Other defects, such as fractures and voids are also apparent at these magnifications.

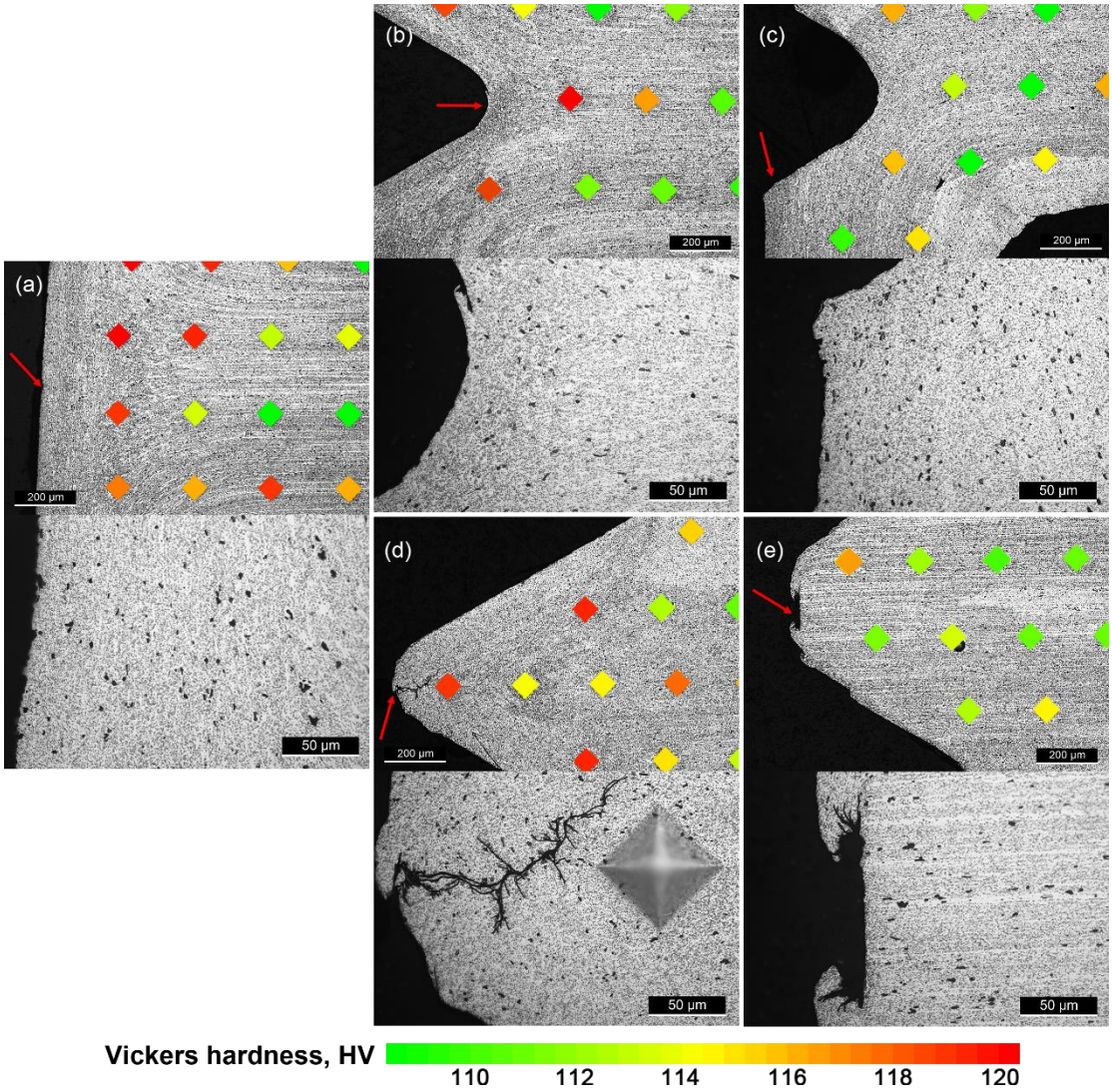

Fig. 6. Microstructure images at higher magnifications. Cases (a) – (e) similar to Fig. 5. Arrows in the upper images indicate locations for images at higher magnification.

3.3 Hardness profiles

The hardness mapping exercise showed increased levels of hardness close to the machined (threaded) surfaces for scenarios in Fig. 5 (a), (b), and (d). This localised

hardening was not as apparent for the scenarios with the cut threads ((c) and (e)). Fig. 7 shows the mean hardness profiles from the thread surfaces for all scenarios. Modest increases in hardness are observed close to the thread surfaces of S1 and S3.

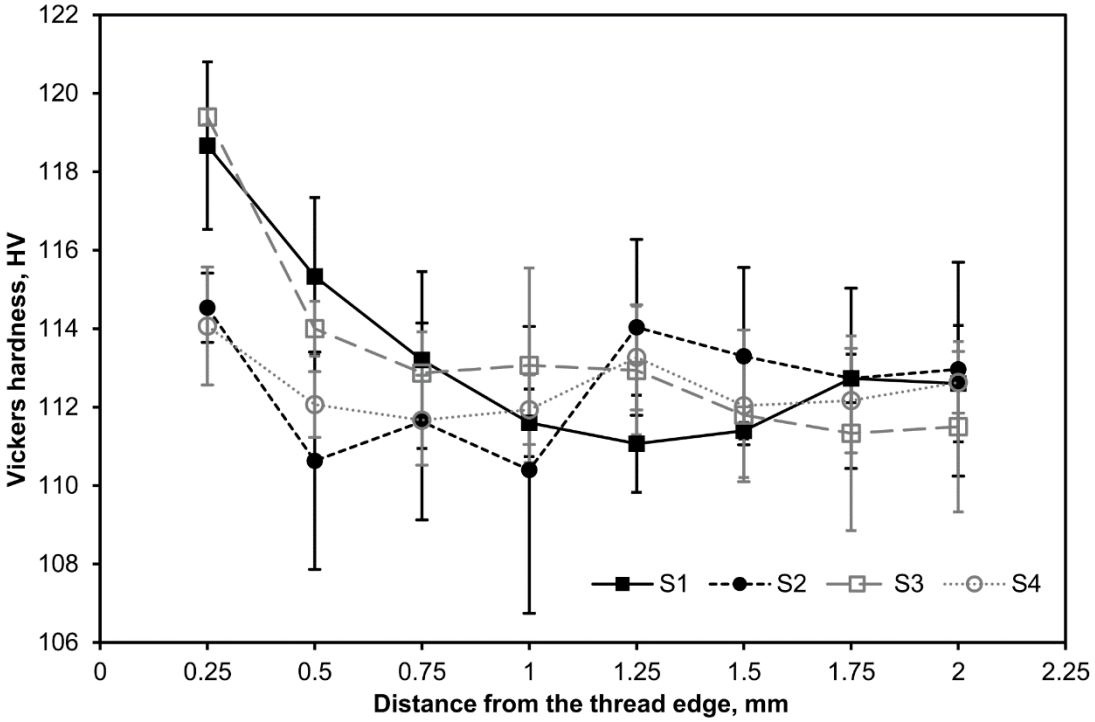

Fig. 7. Mean hardness value from the threaded surface (standard error bars shown).

3.4 Load – deflection results

All samples were load tested to failure and all showed clear and consistent evidence of failure by thread stripping. Fig. 8 shows a typical load-deflection results for each scenario. The load-deflection results were initially linear before reaching a peak load. After peak load, the curves consistently demonstrated a general decreasing trend but with apparent and random load recovery at points. This behaviour is consistent with progressive failure in work-softening materials which has been described by Do et al

[30]. Wittke et al. [18] reported similar progressive failure from their thread stripping tests. Geometry effects due to imperfect metal-to-metal contact and individual thread failures are assumed to account for progressive failure with load recovery at random points.

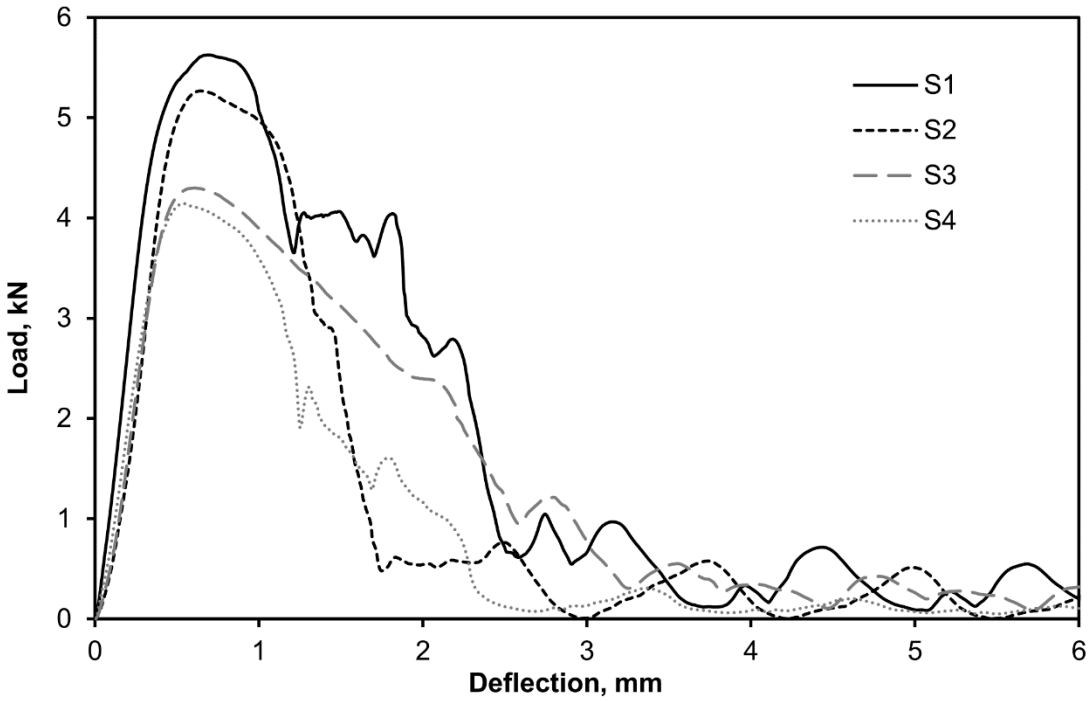

Fig. 8. Representative load-deflection curves for all four scenarios.

In this analysis the threaded joint is assumed to have failed plastically as it reached its peak load-bearing capacity. In all scenarios analysed, the onset of localised yielding (i.e., the deviation from linearity) coincided with the onset of progressive failure in the joint. Table 3 gives a summary of the statistical data for the entire dataset for each scenario. Mean values for failure load and engagement length are plotted in Fig. 9 along with the mean deflection recorded at peak load. Error bars represent the standard errors.

Table 3. Failure loads and engagement lengths – statistical summary.

	Failure loads, kN				Engagement lengths, mm			
	Mean, $\overline{F}_f$	Standard deviation		Standard error, $S_{\overline{F}_f}$	Mean, $\bar{L}_e$	Standard deviation		Standard error, $S_{\bar{L}_e}$
		Abs., S_{Ff}	Rel., C_{Ff}			Abs., S_{Le}	Rel., C_{Le}	
S1	5.20	0.61	0.12	0.25	5.83	0.19	0.03	0.08
S2	4.86	0.90	0.18	0.37	5.67	0.24	0.04	0.10
S3	4.35	0.65	0.15	0.26	2.39	0.15	0.06	0.06
S4	3.86	0.49	0.13	0.20	1.91	0.13	0.07	0.05

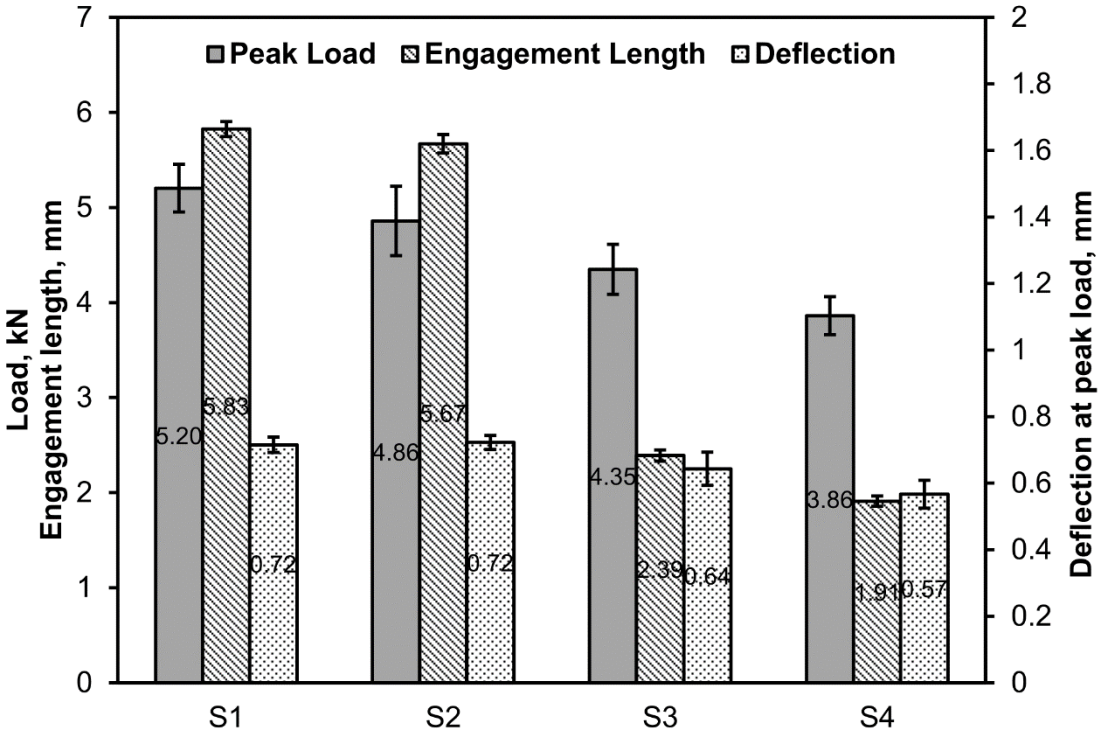

Fig. 9. Peak loads, deflections and engagement lengths of all scenarios.

3.5 Results from the failure analysis

Table 4 summarises the data from the failure analysis. Statistical information on the shear area and shear stress at failure is provided. Furthermore, the principal design factor, n_1, is given. As explained previously, n_1 provides a reliability level of 50% for internal thread stripping failure.

Table 4. Failure analysis and principal design factor – statistical summary.

	Shear area, mm^2			Shear stress at failure, MPa			Design factor
	Mean, $\overline{A}_{\mathrm{n}}$	Standard deviation		Mean, $\overline{\tau}_f$	Standard deviation		Principal factor, n_1
		Abs., $S_{A_{\mathrm{n}}}$	Rel., $C_{A_{\mathrm{n}}}$		Abs., S_{τ_f}	Rel., C_{τ_f}	
S1	108.28	3.57	0.03	48.06	4.89	0.10	3.00

S2	105.43	4.43	0.04	46.09	7.49	0.16	3.13
S3	44.43	2.70	0.06	97.89	9.48	0.10	1.47
S4	35.50	2.46	0.07	108.79	10.84	0.10	1.33

3.6 Reliability results

In order to improve the reliability of the internal thread against thread stripping, a secondary design factor is required based on the corresponding *Z*-value for a given reliability. The reliability levels presented are 95%, 99% and 99.9% with corresponding *Z*-values of -1.65, -2.33, and -3.09, respectively. A *Z*-value of zero gives a design factor of unity, which when combined with the principal design factor relates to a reliability of 50%. Table 5 summarises secondary design factors. Table 6 summarises the overall *FoS* values at each reliability level (using Eqn. (21)).

Table 5. Summary of the secondary design factors.

	R-value	50.0%	95.0%	99.0%	99.9%
	Z-value	0	-1.65	-2.33	-3.09
S1	Secondary design factor, n_2	1.00	1.20	1.31	1.46
S2		1.00	1.37	1.61	2.01
S3		1.00	1.19	1.29	1.43
S4		1.00	1.20	1.30	1.45

Table 6. Summary of the overall Factors of Safety.

	R-value	50.0%	95.0%	99.0%	99.9%
	Z-value	0	-1.65	-2.33	-3.09
S1	Overall Factor of Safety, *FoS*	3.00	3.61	3.94	4.38
S2		3.13	4.28	5.04	6.28
S3		1.47	1.75	1.90	2.10
S4		1.33	1.59	1.73	1.92

4. Discussion

4.1 Failure loads and statistical significance

Although different mean failure loads may be ranked from greatest to least from S1, S2, S3, to S4; the differences needs to be checked for significance. Hence, a two-factor ANOVA was performed across S1 to S4. The categories or factors reviewed were the two drilling and two thread making methods.

Table 7 lists the results of the two-factor ANOVA test. A standard confidence level of 95% was set as the threshold for significance (that is, $p < 0.05$ or $F > F_{crit}$). With a *p*-value of 0.003, the observed increase in failure loads due to friction drilling over twist drilling was statistically significant. With a *p*-value of 0.148, the apparent increase in failure loads attributed to thread forming over thread cutting seemed statistically insignificant. However, it should be recognised that the ANOVA analysis only considers differences in mean values in the dataset. The reliability analysis that follows does show clear benefits of thread forming. In addition, with *p*-value of 0.80 the interaction between drilling and thread manufacture was found to be statistically

insignificant.

Table 7. Two-factor ANOVA results of the failure loads for S1, S2, S3, and S4.

Variation factor	F	F_{crit}	p-value	$p < 0.05$
Drilling method	11.23	4.35	0.003	Yes
Tapping method	2.26	4.35	0.148	No
Interaction	0.066	4.351	0.800	No

4.2 Significance tests of hardness maps

Single-factor ANOVA tests were performed between the two groups of hardness values for each scenario presented in Fig. 5. The two groups considered in each scenario were indents adjacent (0.25mm and 0.5mm) from the thread surfaces and the remaining indents in the parent metal for that scenario. The purpose of this test was to establish if the apparent increase in local hardness level around the thread surfaces were statistically significant compared to the hardness of the parent metal, and to test the depth of the hardened layer with significant increases in the hardness values. The null hypothesis is that the hardness values adjacent to the hole are approximately equal to the nominal hardness (111HV) in the parent metal as provided in Table 1.

Table 8 shows that, when compared to the parent metal, S1 had significantly higher hardness to a depth of 0.5mm; S2 had no significant increase in hardness; S3 had significantly higher hardness to a depth of 0.25mm; and S4 had no significant increase

in hardness.

By comparing the hardness depths to the flow lines in Fig. 5, the depths of hardness correspond to the TMAZ regions (TMAZ regions are identifiable as the places where the flow lines diverge from being parallel). Both friction drilling and thread forming processes increased hardness (either separately or in joint process) around the threaded surfaces. The thread cutting processes did not promote hardness and in the case of S2 appeared to remove the hardened region created by the friction drilling process. Friction drilling and thread forming used in combination (case S1) showed the largest region of hardening around the threads.

Table 8. Significance results for hardness at depths of 0.25mm and 0.5mm from the threaded surfaces.

Significance ($p < 0.05$)	S1	S2	S3	S4
0.25mm from the hole edge	0.000493 (Yes)	0.846091 (No)	0.001098 (Yes)	0.58654 (No)
0.5mm from the hole edge	0.011999 (Yes)	0.284984 (No)	0.859236 (No)	0.568413 (No)

Although the hardness increase due to the forming processes is statistically significant (clear shown from the data) they are modest (maximum hardness of 125HV over the baseline of 111HV). This is not surprising, considering that 6082-T6 is an age

hardening wrought alloy and does not exhibit high work hardening capability. The modest work hardening of this material is in-line with expectations. An important finding from the microstructure analysis is that the distribution of precipitates was consistent, which suggests that the temperatures experienced in the HAZ during the friction drilling process were insufficient to cause dissolution. Temperatures must have been below the solvus temperature 550^{o}C or had insufficient time at peak temperature to affect the distribution of β-Mg_2Si precipitates. Furthermore, there is little evidence of recrystallization and grain coarsening occurring. As stated, small additions of Cr and Mn retard the recrystallization in 6082 alloy.

Hamzawy et al. [16] reported temperatures for friction drilled 6082-T6 in the range of 220ºC to 380ºC. Given that the friction drilling process is a quick in-out drilling process with no dwell time then it is reasonable to propose that the thermal conditions may have limit effects on the T6 temper.

A reduction in ductility with temperature affects the formability of 6082-T6 [31] and this is the probable cause of the fissures in the bushings of the friction drilled holes.

4.3 Design factors and reliability

The calculated shear stresses at failure (Table 4) were, on average, lower in the friction drilling process than in the subtractive drilling processes. The mean values of failure stresses were approximately halved by the friction drilling cases. This significant reduction in failure stress cannot be attributed to a change in the material properties as we have clear evidence that no softening had taken place. Hence the

lower failure stresses are attributed to geometry factors in the friction drilling and thread forming processes. The geometries of the exploded petals were highly irregular and non-ideal. Fissures between the petals and the natural curvature of the petals would have reduced the contact area. Points of high localised stress would have existed. However, the principal design factor, n_1, proposed in this study, accounts for these geometrical imperfections. It is noted that the principal design factors for the friction drilling processes are more than double the corresponding principal factors for the twist drilling processes.

As explained in the derivation, the principal design factor is a baseline *FoS* that gives a reliability of only 50%. Hence, at this baseline there is no margin of error. The secondary design factor, n_2, is required to give higher reliability. The overall *FoS* is provided by getting the product of n_1 and n_2. An important point to discuss is the difference in overall *FoS* trends between S1 and S2 at the higher reliability levels ($\geq$ 95%). The differences in mean failure loads due to the change in thread manufacturing processes were initially shown to be statistically insignificant, which meant that the data showed no difference based on analysis of mean values alone. The principal design factors, n_1, are approximately the same for S1 and S2, leading to the conclusion that at R = 50% the overall *FoS* are 3.00 for S1 and 3.13 for S2. However, S2 showed a larger standard deviation in the failure stresses when compared to S1 (the $c_{\tau f}$ = 0.10 for S1 and $c_{\tau f}$ = 0.16 for S2). This lack of parity in standard deviations between S1 and S2 cannot be attributed to standard deviations in the thread engagement lengths, which were low and close to parity. The non-equal variances in

the stress values could only be attributed to other factors such as the addendum truncation and internal defects as shown in Fig. 5 and Fig. 6. An important discovery in this analysis is that statistical significance testing based on mean values provides necessary but insufficient information to fully assess the reliability of the threads' performance. The standard deviation in the dataset of the threads' performance must be included and this is the case with the reliability analysis.

How the difference in results between S1 and S2 impacted on the performance only becomes apparent at higher levels of reliability (≥ 95%). For example, at R = 99.9% the overall *FoS* are 4.38 for S1 and 6.28 for S2, which would lead to a lower load rating for S2 compared S1 to achieve the same level of reliability. Hence, the combination of friction drilling and thread cutting (S2) is to be avoided. Friction drilling and thread forming (S1) is recommended since it gave the most reliable performance.

4.4 Load rating for high reliability

Budynas and Nisbett [3] presented Shigley's classic approach to dealing with a stochastic calculation with normal variance in the materials strength and normal variance expected in the applied load. This is an inference problem where two normal distributions combine to give a third normal distribution based on margin of safety.

Shigley's approach is adapted here to give a secondary design factor as follows:

$$n_2 = \frac{1+\sqrt{1-\left(1-z^2C_{\tau_f}^2\right)\left(1-z^2C_{\tau}^2\right)}}{1-z^2C_{\tau_f}^2}. \tag{22}$$

Here, Z, and the coefficient of variance, $C_{\tau f}$, has the same definition as used previously. If a load, P, is varies normally, then it will have a mean value, $\bar{P}$, and a coefficient of

variance, C_P. Eqn. (22) requires an additional coefficient of variance for the applied stress, C_τ. This value can be estimated using the following expression (covariance is conservatively ignored in Shigley's analysis):

$$C_\tau = \sqrt{C_{A_n}^2 + C_P^2}. \tag{23}$$

The coefficient of variance for shear area, C_{An} (provided in Table 4), is directly applicable in this case and the coefficient of variance for the load, C_P, should be known to the designer. The applied stress to achieve a given reliability (based on the corresponding *Z*-value) is provided as

$$\tau = \frac{\tau_y}{n_1 n_2}. \tag{24}$$

Where n_1 is the principal design factor (provided in Table 4) and τ_y is the shear yield strength (Eqn. (16)). Finally, the new load rating for a given *Z*-value is given by

$$\bar{P} = \tau A_n. \tag{25}$$

A demonstration is given using the data provided in this manuscript and a load coefficient of variance, C_P = 0.1 or 10%. Table 9 shows average loads, $\bar{P}$, rated at 99.9% reliability.

Table 9. Load rating for a reliability of 99.9% with load variance C_P = 0.1.

	R-value	*Z*-value	C_P	*A*n, mm^2	C_{An}	C_τ	n_1	n_2	$\bar{P}$, kN
S1	99.9%	-3.09	0.10	108.28	0.03	0.11	3.00	1.60	3,253
S2	99.9%	-3.09	0.10	105.43	0.04	0.11	3.13	2.11	2,301
S3	99.9%	-3.09	0.10	44.43	0.06	0.12	1.47	1.60	2,718
S4	99.9%	-3.09	0.10	35.50	0.07	0.12	1.33	1.63	2,374

S1 has the highest load rating. Otherwise, S2 is lowest rated joint at that same

reliability level. Indeed, the load rating for S2 (friction drilling and thread cutting) is lower than both twist-drilled options (S3 and S4). Hence, reinforcing the fact that thread forming should only be used in conjunction friction drilling when creating a threaded hole.

5. Conclusion

The overall aims of this study were to investigate the mechanical performance of threaded holes in thin section 6082-T6 aluminium alloy and to provide Factor of Safety information for designers. To fulfil these aims, four combinations of the threaded holes were manufactured based on different drilling and thread making methods. A detailed test procedure to determine the axial load bearing capacity in threaded joints was presented. The compression test presented here expands significantly on international standard tests [6,7]. A detailed test program was performed to generate statistical data on the thread performance. Results demonstrated that the threaded holes made by friction drilling and thread forming were able to achieve 35% increase in peak load when compared to threaded holes made by conventional twist drilling.

Hardness testing showed modest increases in hardness from 111HV to 125HV within 0.5mm distance due to friction drilling and thread forming. The increase was attributed to work hardening and no evidence of precipitation dissolution was found (suggesting that friction drilling temperatures were below the solvus temperature for this alloy). The increase in average load bearing capacity in friction drilled holes over

conventional drilled ones was shown to be statistically significant. The benefits of the thread forming process over the thread cutting (or taper tapping) process only became apparent after a detailed reliability analysis was performed. Hence, the processes recommended to avoid thread stripping in axially loaded joints are friction drilling followed by thread forming. Factors of safety selected for these joint types that are within the range from 3.61 to 4.38 will give between 95% and 99.9% reliability against thread stripping.

The investigation developed here has focussed on a singular hole size (M8x1.5) within a single material (aluminium alloy 6082-T6) of single thickness (1.5mm). Friction drilling is currently applied to many other application areas with differing material selection, hole, and thickness requirements. It is proposed that the testing processes presented herein can be applied to cover all possible scenarios that involve friction drilling to produce threaded holes.

Acknowledgments

This research has been supported by the INTERREGVA (Project ID: IVA5055, Project Reference Number: 047). The North West Centre for Advanced Manufacturing (NW CAM) project is supported by the European Union's INTERREG VA Programme, managed by the Special EU Programmes Body (SEUPB). The views and opinions in this document do not necessarily reflect those of the European Commission or the Special EU Programmes Body (SEUPB). If you would like further information about NW CAM please contact the lead partner, Catalyst, for details. The authors declare that there are no conflicts of interest.

References

[1] J.A. van Geffen, Methods and apparatuses for forming by frictional heat and pressure holes surrounded each by a boss in a metal plate or the wall of a metal tube, US Patent 4,175,413A, 1979.

[2] R. Kumar, N.R.J. Hynes, Thermal drilling processing on sheet metals: A review, Int. J. Light. Mater. Manuf. 2 (2019) 193–205. doi:10.1016/j.ijlmm.2019.08.003.

[3] R. Budynas, J.K. Nisbett, Shigley’s Mechanical Engineering Design, 10th ed., McGraw-Hill Education, 2014. doi:10.1007/s13398-014-0173-7.2.

[4] E. Oberg, F.D. Jones, H.L. Horton, H.H. Ryffel, Machinerys Handbook, 26th ed., Indutrial Press Inc, New York, 2000. doi:10.1039/c3ja50313e.

[5] R.C. Juvinall, K.M. Marshek, Fundamentals of Machine Component Design,

5th ed., John Wiley & Sons, Inc., 2012.

[6] International Organization for Standardization, Mechanical properties of fasteners made of carbon steel and alloy steel Part 2 : Nuts with specified property classes - Coarse thread and fine pitch thread, ISO 898-22012. BS EN ISO (2012) 1–30.

[7] American Society for Testing and Materials, ASTM F606/F606M -16: Standard Test Methods for Determining the Mechanical Properties of Externally and Internally Threaded Fasteners , Washers , Direct Tension Indicators , and Rivets, (2016) 1–19. doi:10.1520/F0606.

[8] S.F. Miller, R. Li, H. Wang, A.J. Shih, Experimental and Numerical Analysis of the Friction Drilling Process, J. Manuf. Sci. Eng. (2006). doi:10.1115/1.2193554.

[9] S.F. Miller, J. Tao, A.J. Shih, Friction drilling of cast metals, Int. J. Mach. Tools Manuf. 46 (2006) 1526–1535. doi:10.1016/j.ijmachtools.2005.09.003.

[10] S.F. Miller, A.J. Shih, Thermo-mechanical finite element modeling of the friction drilling process, J. Manuf. Sci. Eng. Trans. ASME. 129 (2007) 531–538. doi:10.1115/1.2716719.

[11] H.M. Chow, S.M. Lee, L.D. Yang, Machining characteristic study of friction drilling on AISI 304 stainless steel, J. Mater. Process. Technol. 207 (2008) 180–186. doi:10.1016/j.jmatprotec.2007.12.064.

[12] C. Ozek, Z. Demir, Investigate the Friction Drilling of Aluminium Alloys According to the Thermal Conductivity, TEM J. 2 (2013) 93–101.

http://www.tem-journal.com/archives/vol2no1.html.

[13] N.R.J. Hynes, R. Kumar, Process optimization for maximizing bushing length in thermal drilling using integrated ANN-SA approach, J. Brazilian Soc. Mech. Sci. Eng. 39 (2017) 5097–5108. doi:10.1007/s40430-017-0820-y.

[14] A.A. Eliseev, S. V. Fortuna, E.A. Kolubaev, T.A. Kalashnikova, Microstructure modification of 2024 aluminum alloy produced by friction drilling, Mater. Sci. Eng. A. 691 (2017) 121–125. doi:10.1016/j.msea.2017.03.040.

[15] S.F. Miller, P.J. Blau, A.J. Shih, Microstructural alterations associated with friction drilling of steel, aluminum, and titanium, J. Mater. Eng. Perform. 14 (2005) 647–653. doi:10.1361/105994905X64558.

[16] N. Hamzawy, M. Khedr, T.S. Mahmoud, I. EI-Mahallawi, T.A. Khalifa, Investigation of Temperature Variation During Friction Drilling of 6082 and 7075 Al-Alloys, in: A. Tomsett (Ed.), Light Met. 2020, Springer International Publishing, Cham, 2020: pp. 471–477.

[17] G. Urbikain, J.M. Perez, L.N. López de Lacalle, A. Andueza, Combination of friction drilling and form tapping processes on dissimilar materials for making nutless joints, Proc. Inst. Mech. Eng. Part B J. Eng. Manuf. (2018). doi:10.1177/0954405416661002.

[18] P. Wittke, M. Teschke, F. Walther, Mechanical characterization of friction drilled internal threads in AZ91 profiles, Int. J. Adv. Manuf. Technol. 99 (2018) 3111–3122. doi:10.1007/s00170-018-2698-y.

[19] D. Trimble, H. Mitrogiannopoulos, G.E. O'Donnell, S. McFadden, Friction stir

welding of AA2024-T3 plate - The influence of different pin types, Mech. Sci. 6 (2015) 51–55. doi:10.5194/ms-6-51-2015.

[20] Y. Huang, Y. Xie, X. Meng, J. Li, Atypical grain coarsening of friction stir welded AA6082-T6: Characterization and modeling, Mater. Sci. Eng. A. 740–741 (2019) 211–217. doi:10.1016/j.msea.2018.10.109.

[21] H. Wu, Y.C. Chen, D. Strong, P. Prangnell, Stationary shoulder FSW for joining high strength aluminum alloys, J. Mater. Process. Technol. 221 (2015) 187–196. doi:10.1016/j.jmatprotec.2015.02.015.

[22] Y. Huang, T. Huang, L. Wan, X. Meng, L. Zhou, Material flow and mechanical properties of aluminum-to-steel self-riveting friction stir lap joints, J. Mater. Process. Technol. 263 (2019) 129–137. doi:10.1016/j.jmatprotec.2018.08.011.

[23] British Standards Institution, BS EN 755-2:2016: Aluminium and aluminium alloys - Extruded rod/bar, tube and profiles - Part 2: Mechanical properties, (2016). https://bsol.bsigroup.com (accessed May 4, 2020).

[24] American Society for Testing and Materials, Standard Hardness Conversion Tables for Metals Relationship Among Brinell Hardness, Vickers Hardness, Rockwell Hardness, Superficial Hardness, Knoop Hardness, and Scleroscope Hardness, Standard. E140 (2019) 1–21. doi:10.1520/E0140-12R19E01.1.6.

[25] C.D. Marioara, S.J. Andersen, J. Jansen, H.W. Zandbergen, Atomic model for GP-zones in a 6082 Al-Mg-Si system, Acta Mater. 49 (2001) 321–328. doi:10.1016/S1359-6454(00)00302-5.

[26] British Standards Institution, BS EN ISO 6507‑1：2018 BSI Standards

Publication Metallic materials - Vickers hardness test, (2018). https://bsol.bsigroup.com/ (accessed May 4, 2020).

[27] H.H. Ku, Notes on the use of propagation of error formulas, J. Res. Natl. Bur. Stand. Sect. C Eng. Instrum. 70C (1966) 263. doi:10.6028/jres.070c.025.

[28] K.O. Pedersen, O.G. Lademo, T. Berstad, T. Furu, O.S. Hopperstad, Influence of texture and grain structure on strain localisation and formability for AlMgSi alloys, J. Mater. Process. Technol. 200 (2008) 77–93. doi:10.1016/j.jmatprotec.2007.08.040.

[29] British Standards Institution, BS ISO 68-1:1998+A1:2020: ISO general purpose screw threads — Basic profile, Part 1: Metric screw threads, (2020). https://bsol.bsigroup.com/ (accessed May 6, 2020).

[30] X.N. Do, A. Ibrahimbegovic, D. Brancherie, Combined hardening and localized failure with softening plasticity in dynamics, Coupled Syst. Mech. 4 (2015) 115–136. doi:10.12989/csm.2015.4.2.115.

[31] I. Torca, A. Aginagalde, J.A. Esnaola, L. Galdos, Z. Azpilgain, C. Garcia, Tensile behaviour of 6082 aluminium alloy sheet under different conditions of heat treatment, temperature and strain rate, Key Eng. Mater. 423 (2010) 105–112. doi:10.4028/www.scientific.net/KEM.423.105.